



# HHS Public Access

Author manuscript

*J Mol Biol.* Author manuscript; available in PMC 2020 December 16.

Published in final edited form as:

*J Mol Biol.* 2016 February 13; 428(3): 590–602. doi:10.1016/j.jmb.2016.01.011.

## New Ligand Binding Function of Human Cerberus and Role of Proteolytic Processing in Regulating Ligand–Receptor Interactions and Antagonist Activity

Senem Aykul, Erik Martinez-Hackert

, Michigan State University, East Lansing, MI 48824-1319, USA

### Abstract

Cerberus is a key regulator of vertebrate embryogenesis. Its biological function has been studied extensively in frog and mouse embryos. Its ability to bind and antagonize the transforming growth factor- $\beta$  (TGF- $\beta$ ) family ligand Nodal is well established. Strikingly, the molecular function of Cerberus remains poorly understood. The underlying reason is that Cerberus is a complex, multifunctional protein: It binds and inhibits multiple TGF- $\beta$  family ligands, it may bind and inhibit some Wnt family members, and two different forms with distinct activities have been described. In addition, sequence homology between frog and mammalian Cerberus is low, suggesting that previous studies, which analyzed frog Cerberus function, may not accurately describe the function of mammalian Cerberus. We therefore undertook to determine the molecular activities of human Cerberus in TGF- $\beta$  family signaling. Using purified proteins, surface plasmon resonance, and reporter gene assays, we discovered that human Cerberus bound and inhibited the TGF- $\beta$  family ligands Activin B, BMP-6, and BMP-7, but not the frog Cerberus ligand BMP-2. Notably, full-length Cerberus successfully blocked ligand binding to type II receptors, but the short form was less effective. In addition, full-length Cerberus suppressed breast cancer cell migration but the short form did not. Thus, our findings expand the roles of Cerberus as TGF- $\beta$  family signaling inhibitor, provide a molecular rationale for the function of the N-terminal region, and support the idea that Cerberus could have regulatory activities beyond direct inhibition of TGF- $\beta$  family signaling.

### Keywords

Cerberus; SPR; signaling; cancer; TGF- $\beta$

### Introduction

Cerberus is a secreted antagonist of transforming growth factor- $\beta$  (TGF- $\beta$ ) family signaling that belongs to the DAN (differential screening-selected gene aberrative in neuroblastoma) family of cystine knot proteins [1,2]. It plays an important role in head formation and

**Correspondence to Erik Martinez-Hackert:** Michigan State University, Biochemistry Room 509, 603 Wilson Road, East Lansing, MI 48824-1319, USA. emh@msu.edu.

Appendix A. Supplementary data

Supplementary data to this article can be found online at <http://dx.doi.org/10.1016/j.jmb.2016.01.011>.

cardiogenesis during vertebrate embryonic development [3–8]. Overexpression of frog Cerberus (xCer) in frog embryos induced formation of ectopic heads [3,9], and Cerberus knockdown in mouse embryonic stem cells prevented cardiac lineage specification [7]. Beyond embryogenesis and cardiogenic progenitor cells, Cerberus functions are not known. However, mutations in the Cerberus gene are well correlated with an increased risk of low bone mineral density (BMD) in premenopausal women and osteoporosis in postmenopausal women [10–12]. Significantly, how Cerberus regulates head formation, cardiac lineage commitment, and BMD is not well understood because its molecular activities are poorly defined. The common view is that Cerberus is a multifunctional protein that binds and inhibits the TGF- $\beta$  family ligands Nodal, BMP-2, BMP-4, and Activin A, as well as some members of the Wnt family [1,13]; however, contradicting activities have also been reported. For example, frog Cerberus inhibited frog Nodal (Xnr1 and Xnr2), BMP-2, BMP-4, and XWnt8 (frog Wnt8) [1], whereas mouse and human Cerberus only inhibited Nodal [13–15].

A possible reason for the different observations is limited sequence conservation between Cerberus from different species [13,15]. Human and mouse Cerberus, respectively, only share 35.7% and 33.8% sequence identity with frog Cerberus. Even between human and mouse Cerberus, sequence identity is only 67.2% [2,15]. Notably, sequence identity in the C-terminal cystine knot domain is approximately 50% between the mammalian and the frog species, whereas conservation in the N-terminal half of the sequence is nearly negligible. In addition, two forms of frog Cerberus with potentially distinct functions have been described [1]. A long form (xCer-L) inhibited Xnr2, BMP-2, BMP-4, and XWnt8, whereas a short form (xCer-S), which is likely generated by proteolytic processing of xCer-L, only inhibited Xnr2 [1]. Taken together, these findings indicate that the molecular functions of mammalian Cerberus need to be defined. Knowing which signaling pathways mammalian Cerberus regulates and how the long and short forms of Cerberus differ is critically important for elucidating the cellular programs that lead to head formation in developing embryos, to differentiation of mouse cardiogenic progenitors, and to low BMD and osteoporosis in women that carry the mutant Cerberus alleles.

To clarify the function of human Cerberus in TGF- $\beta$  family signaling, we investigated its ligand binding specificity and its ability to inhibit signaling. Using purified proteins and surface plasmon resonance (SPR), we discovered three new TGF- $\beta$  family ligands that bind human Cerberus with high affinity: Activin B, BMP-6, and BMP-7. Using SPR and reporter gene assays, we showed that human Cerberus prevented type II receptor binding and signaling by these ligands and by Nodal, but not by its putative ligand BMP-2, or Activin A, indicating that the activity of human Cerberus differs from the activity reported for frog Cerberus [1]. Notably, full-length and short-form Cerberus bound and inhibited ligands equivalently, but the two forms differed in their ability to prevent ligand binding to type II receptors, suggesting that the cleavable N-terminal region could play a role in blocking the type II receptor binding surface. In addition, full-length Cerberus profoundly suppressed migration of MDA-MB-231 breast cancer cells, whereas short-form Cerberus did not, suggesting that the different forms of Cerberus could have distinct biological activities, such as regulation of Wnt signaling via the cleavable N-terminal region. Indeed, full-length frog Cerberus (Cer-L) co-immunoprecipitated with the Wnt family ligand XWnt8, but the short form (Cer-S) did not [1]. In conclusion, we have identified new TGF- $\beta$  family signaling

ligands that are antagonized by human Cerberus and we have elucidated molecular and biological activities of full-length and short-form Cerberus.

## Results

### Construct design

Cerberus is widely considered to be a multifunctional protein that inhibits Nodal, bone morphogenetic proteins BMP, Activin A, and Wnt activity; however, conflicting findings regarding its function have been reported [1,13–15]. To clarify the molecular activities of human Cerberus, we expressed a number of constructs as Fc fusion proteins using stably transfected Chinese hamster ovary (CHO) cells, including wild-type Cerberus (wtCer-Fc), mutant Cerberus (mutCer-Fc), and short-form Cerberus (CerS-Fc) (Fig. 1a and b). For wild-type Cerberus, the complete wild-type human sequence was used. For mutant Cerberus, a putative proprotein convertase processing site (Arg82Gly) and an unpaired cysteine were modified (Cys206Ala) [16,17]. For short Cerberus, the sequence between signal peptide and a predicted proprotein convertase processing site was deleted (18–85) and the unpaired cysteine was mutated (Cys206Ala). Cerberus was fused at the C-terminus to the Fc portion of human IgG1 via a 22-amino-acid linker containing a tobacco etch mosaic virus (TEV) cleavage site (Fig. 1b).

Cerberus-Fc fusion proteins were purified from conditioned medium by protein A affinity chromatography followed by size-exclusion chromatography (SEC) (Fig. 1c–e). Preparative SEC showed that wtCer-Fc and CerS-Fc were significantly aggregated, whereas mutCer-Fc was almost free of aggregates (data not shown). Monodisperse peaks corresponding to a dimeric species could be obtained by sequential SEC purification cycles (Fig. 1c). To produce the Fc free forms for SPR and other inhibition studies, we digested purified fusion proteins with TEV. The Fc portion was removed by passing the digested form over a protein A column followed by SEC. Fc free Cerberus, constructs were monodisperse by SEC (Fig. 1d). Cerberus elution volumes corresponded to a dimeric form for the full-length constructs, but the elution volume of the CerS construct appeared to be consistent with a monomeric species (Fig. 1d).

To determine the dimerization state of Cerberus and the role of its unpaired cysteine, we used SDS-PAGE mobility assays. Molecular masses of Cerberus-Fc constructs were ~65–75 kDa under reducing conditions and ~130–150 kDa under non-reducing conditions, as expected for the disulfide-linked Fc fusion proteins (Fig. 1e, FC). The Fc free forms migrated as ~30- to 35-kDa proteins on SDS-PAGE under both reducing and non-reducing conditions, demonstrating that human Cerberus, like its homologs PRDC and NBL1, does not form disulfide-linked homodimers (Fig. 1e, TEV) [16,17]. Notably, glutaraldehyde cross-linking of the purified Fc free Cerberus fractions showed that both full-length and short-form Cerberus, like its homologs PRDC and NBL1, form non-covalent dimers in solution (Fig. 1d) [16,17].

Cerberus constructs migrated with elevated motility on SDS page and both full-length forms contained degradation products. To clarify the contribution of glycosylation and proteolytic cleavage to SDS-PAGE heterogeneity and elevated molecular mass, we digested mutCer

with deglycosylation enzymes (Fig. 1e, DEG). Treatment with PNGase F alone decreased the molecular mass of full-length Cerberus to approximately 30 kDa. Simultaneous treatment with PNGase F and sialidase produced a homogenous band that corresponded to the theoretical molecular mass of full-length Cerberus, which is 28 kDa, indicating that Cerberus is heavily N- and O-glycosylated. Based on SDS-PAGE mobility, the degradation product of full-length Cerberus corresponded approximately to the cloned, short-form Cerberus, indicating that Cerberus can be proteolytically processed and that cleavage occurs at or near the predicted proprotein convertase processing site (Fig. 1e, red star). SEC elution volumes of the short form and the degradation product are the same, indicating that the oligomeric state and apparent molecular weight of the two proteins are the same.

### Ligand binding

Co-immunoprecipitation studies have indicated that frog and/or mouse Cerberus bind Nodal, BMP-2, BMP-4, and possibly Activin A [1,13]. By contrast, we previously showed that, out of seven tested TGF- $\beta$  family ligands, including BMP-2, Activin A, and Nodal, only Nodal bound human Cerberus with significant affinity [1,13,15,18]. To investigate more broadly the ligand binding specificity of human Cerberus, we used a high-throughput, SPR-based binding assay. We captured purified wtCer-Fc on a Biacore sensor chip that was cross-linked with an anti-human Fc antibody and we injected 15 different TGF- $\beta$ -family ligands at a concentration that exceeds physiological levels (80 nM) [19–21]. As expected, most of the tested TGF- $\beta$ -family ligands did not bind Cerberus with appreciable affinities, including Activin A, BMP-2, TGF- $\beta$ 1, TGF- $\beta$ 2, TGF- $\beta$ 3, GDF-1, GDF-3, GDF-8, and BMP-9 (Fig. 2a) [15]. Notably, we discovered three new ligands that bind human Cerberus in addition to Nodal: Activin B, BMP-6, and BMP-7.

Frog Cerberus exists in a long form and a processed, short form. Short-form Cerberus is thought to bind and inhibit Nodal, but not other ligands [1]. To evaluate the role in ligand binding of the proprotein convertase cleavable N-terminal region and of the unpaired cysteine (Cys206), we determined the ligand binding profiles of CerS and mutCer using the high-throughput, SPR-based binding assay. We captured purified CerS-Fc and mutCer-Fc on a Biacore sensor chip and we injected 15 different ligands at 80 nM concentration as we did for wtCer-Fc (Fig. 2b–d). Intriguingly, we found that ligand binding by CerS-Fc and mutCer-Fc was not significantly different from wtCer-Fc for BMP-6 and BMP-7, whereas the dissociation rate for Activin B was approximately 10-fold faster with wtCer-Fc. Nevertheless, Cerberus–Activin B equilibrium dissociation constants were low, ranging from 20 to 100 pM. Thus, the cleavable N-terminus and the unpaired cysteine of human Cerberus do not appear to have a major, direct role in ligand binding affinity or specificity.

To determine the binding affinity of the newly discovered Cerberus ligands Activin B, BMP-6, and BMP-7, we captured wtCer-Fc, mutCer-Fc, and CerS-Fc on a Biacore sensor chip and we injected a concentration series for each one of these three ligands (Fig. 3, Fig. S1, and Table 1). wtCer-Fc bound Activin B with affinities that are comparable to refolded Nodal [ $k_a = 2.3 \times 10^6$  ( $M^{-1} s^{-1}$ ),  $k_d = 2.2 \times 10^{-6}$  ( $s^{-1}$ ), and  $K_d = 0.096$  nM] (Fig. 3) [15]. The association rate was very fast and the dissociation rate was very slow, as expected for a very strong, picomolar interaction. Binding of BMP-6 and BMP-7 was significantly weaker,

but complexes were stable, as indicated by the low-nanomolar equilibrium dissociation constant ( $K_d = 19$  nM and 17 nM, respectively; Fig. 3 and Fig. S1). Even at this comparatively weak affinity, BMP-6 and BMP-7 bound Cerberus with several orders of magnitude higher affinity than the frog Cerberus ligands BMP-2 [15]. Notably, while mutCer-Fc and CerS-Fc bound ligands with association rates that were similar to those of wtCer-Fc, the dissociation rates were marginally slower, suggesting that mutCer-Fc and CerS-Fc complexes are more stable (Fig. 3 and Table 1). In sum, Nodal and Activin B are the highest-affinity ligands of human Cerberus; however, human Cerberus also binds BMP-6 and BMP-7 with significant affinities.

### Mechanism of inhibition

Cerberus blocked binding of Nodal to its type I and type II receptors [1,13,15]. Inhibition of Nodal binding to the type II receptors ActRIIA and ActRIIB was more efficient than to BMPRII [15]. To validate the mechanism of Cerberus inhibition and to examine its potential for differential regulation, we investigated the effect of the different Cerberus constructs on ligand binding to the type II receptors ActRIIA, ActRIIB, and BMPRII. Type II receptor-Fc fusion proteins were captured on a Biacore sensor chip that was cross-linked with an anti-human Fc antibody. Activin B and BMP-6 (10 nM and 80 nM, respectively) were preincubated with Fc free Cerberus at concentrations ranging from 0 nM to 4000 nM. Preassembled ligand–Cerberus complexes were injected over the captured receptors (Fig. 4). In this format, Cerberus must be Fc free to avoid binding of Fc to the anti-human Fc antibody cross-linked sensor chip.

As expected, Cerberus prevented Activin B and BMP-6 binding to ActRIIA-Fc, ActRIIB-Fc, and BMPRII-Fc in a concentration-dependent manner (Fig. 4). Inhibition kinetics indicated that Cerberus is a competitive inhibitor of the ligand–type II receptor interaction, further supporting the conclusion that Cerberus binds ligands also by covering the type II receptor binding site [15]. However, the different Cerberus constructs did not inhibit ligands equivalently. wtCer strongly inhibited the low picomolar ( $K_d \approx 0.01$  nM) interaction between Activin B and the type II receptor ActRIIA ( $IC_{50}$  of 26 nM; Fig. 4 and Table 2), whereas mutCer and CerS were less effective ( $IC_{50}$  of 40 nM and 261 nM, respectively); 50 nM wtCer reduced binding of Activin B to ActRIIA by approximately 60% (Fig. 4). By contrast, 50 nM CerS only reduced binding of 10 nM Activin B to ActRIIA by approximately 10%. This trend extends to inhibition of ligand binding to ActRIIB-Fc (data not shown) and BMPRII-Fc (Fig. 4 and Table 2), as well as Nodal (Fig. S2). However, as Activin B and BMP-7 binding to BMPRII is weaker than to ActRIIA, inhibition of ligand binding to BMPRII is more effective for all Cerberus forms against these two ligands. By contrast, Cerberus does not completely block binding of Nodal to BMPRII (Fig. S2). By itself, Cerberus does not bind ActRIIA, ActRIIB, or BMPRII. Taken together, our findings indicate that all Cerberus constructs inhibit ligand binding to type II receptors. mutCer is as effective as wtCer, indicating that the unpaired cysteine and/or the single point mutation in the proprotein convertase processing site do not contribute significantly to inhibition of the ligand–type II receptor interaction. By contrast, the cleavable N-terminus appears to have a more direct role in blocking ligand binding to type II receptors, as an approximately 10-fold higher concentration of the short form was needed to inhibit receptor binding. We did not

evaluate type I receptor inhibition, as we currently do not know which type I receptors are bound by Activin B, BMP-6, or BMP-7.

### Signaling inhibition

As Cerberus inhibited the ligand–type II receptor interaction and inhibited Nodal signaling *in vivo* [15,22–24], we hypothesized that Cerberus could also inhibit signaling by its newly identified ligands. To test this hypothesis, we used a luciferase reporter gene assay. We transfected A-204 cells with control plasmid pGL4.74 [hRluc] and the SMAD3 responsive reporter plasmid pGL4.48 [luc2P/SBE] or HepG2 cells with the same control plasmid and the SMAD1/5/9 responsive reporter plasmid pGL3 [luc2P/BRE] [25,26]. Transfected A-204 cells were treated with 0.8 nM Activin A or Activin B, and HepG2 cells were treated with 0.8 nM BMP-2 or BMP-6 [25,26]. Both Activin A and Activin B induced luciferase expression with the SMAD3 reporter, and both BMP-2 and BMP-6 induced luciferase expression with the SMAD1/5/9 reporter, as expected (Fig. 5). Addition of wtCer-Fc inhibited Activin B and BMP-6 signaling in a concentration-dependent manner, but not Activin A or BMP-2. mutCer-Fc and CerS-Fc also inhibited Activin B and BMP-6 signaling, and their efficacy was similar to wtCer-Fc. To determine whether the Fc moiety had an impact on signaling inhibition, we performed this assay with the Fc free wtCer form. Its effect on signaling was comparable to wtCer-Fc (Fig. 5).

Using the luciferase reporter gene expression data, we calculated  $IC_{50}$  for inhibition with the different Cerberus constructs. Overall,  $IC_{50}$  values are in agreement with, but are not identical with,  $IC_{50}$  values determined by SPR (Figs. 3–5 and Table 2). One possible reason for the observed differences is that, with SPR, we determined an  $IC_{50}$  relative to individual receptors. By contrast, in the cell-based assay, we determined an  $IC_{50}$  that combines the contributions of all the receptors expressed on the cell surface. As Activin B and BMP-6 interact, at least, with ActRIIA, ActRIIB, and BMPRII, an  $IC_{50}$  determined by SPR should be similar but cannot be identical with an  $IC_{50}$  determined in a whole cell context, where all three receptors are present at the same time.

### Wound healing

Long-form (xCer-L) and short-form (xCer-S) frog Cerberus have distinct biological activities [1]. As full-length human Cerberus fused to Fc (wtCer-Fc) inhibited migration of MDA-MB-231 breast cancer cells [15], we undertook to evaluate, using a wound healing assay, how different human Cerberus-Fc fusion constructs inhibit MDA-MB-231 migration (Fig. 6a and b). We plated MDA-MB-231 breast cancer cells in an Ibidi culture insert. When cells reached 80% confluence, we removed the insert and replaced culture medium with fresh medium containing 2.5  $\mu$ g/ml mitomycin C with or without 17.8 nM wtCer-Fc, mutCer-Fc, or CerS-Fc. As expected, the 500- $\mu$ m gap created by the culture insert completely closed within 24 h in untreated cells (Fig. 6a and b, control). By contrast, wtCer-Fc completely prevented wound closure, confirming its ability to suppress MDA-MB-231 migration (Fig. 6a and b, wtCer-Fc) [15]. mutCer-Fc also had a strong effect on migration, although it was slightly less effective than wtCer-Fc (Fig. 6a and b, mutCer-Fc). Strikingly, CerS-Fc lost the ability to suppress migration, allowing greater than 75% wound closure relative to wtCer-Fc (Fig. 6a and b, CerS-Fc). To ascertain that the unpaired cysteine had no

direct role in suppressing MDA-MB-231 migration, we generated a construct that only carried the C206A mutation. This construct was as effective as wtCer-Fc (data not shown), demonstrating that the unpaired cysteine does not have a prominent role Cerberus inhibition of breast cancer cell migration. Importantly, the Fc domain did not have an effect on Cerberus activity, as the different Fc free Cerberus constructs closely paralleled the effect of the corresponding Fc fusion forms (Fig. S4). Taken together, these findings suggest that the N-terminus of human Cerberus is critical for suppressing MDA-MB-231 cell migration and indicate that the long and short forms could have distinct biological activities, even if ligand binding affinities or the ability to inhibit signaling of the Fc fusion constructs is not significantly different.

## Discussion

Cerberus is a secreted regulator of TGF- $\beta$  family signaling that has multiple antagonist activities and that exists in two functionally distinct forms. Which TGF- $\beta$  family signaling pathways human Cerberus regulates and how the two forms function is poorly understood, as the molecular activities of human Cerberus are yet to be properly defined. As Cerberus is an important regulator of key developmental processes, including head formation and cardiogenesis, and as human Cerberus may play a critical role in adult bone homeostasis, elucidating its function is of considerable biological and biomedical significance. Thus, our goal here was to determine the TGF- $\beta$  family ligand binding specificity of human Cerberus and to elucidate the function of the N-terminal region, which has a proprotein convertase recognition sequence and is cleaved to produce a processed form with a distinct activity.

Previous studies have indicated that frog Cerberus is an antagonist of the TGF- $\beta$  family ligands Nodal, BMP-2, and BMP-4 [1]. These findings have encouraged the consensus view that every Cerberus from every species is a “BMP” antagonist [13,27]. However, while we and others have confirmed that human and mouse Cerberus bound and inhibited Nodal, we also discovered that human Cerberus did not bind or inhibit BMP-2 [13,15]. On the other hand, frog Cerberus antagonizes multiple TGF- $\beta$  family ligands, suggesting that members of the Cerberus family could be promiscuous TGF- $\beta$  family ligand inhibitors. To better understand the scope of human Cerberus function, we examined whether it could also bind and inhibit multiple TGF- $\beta$  family ligands. In addition to Nodal, we found that human Cerberus bound Activin B, BMP-6, and BMP-7 with high affinity (Figs. 2 and 3 and Table 1), but not BMP-2, or other close homologs of Activin B, including Activin A. Notably, Activin A and Activin B are often considered to be functionally equivalent, and Nodal and Activin A are often used interchangeably in biological assays. The exquisite specificity of the Cerberus–Activin B and Cerberus–Nodal interactions suggests, however, that Activin A could perform biological functions while Cerberus is proximally expressed in order to inhibit Nodal or Activin B signaling. In sum, we show that TGF- $\beta$  family signaling regulation by human Cerberus is restricted to a small and specific group of ligands that is different from that reported for frog Cerberus [13,15]. Notably, we suggest that inhibition of Activin B by human Cerberus could play a role in regulating BMD [28].

When frog Cerberus was first characterized, two different forms of the gene product were observed [1]. Animal cap cells secreted a soluble protein of 46,000 kDa and a minor form of

33,000 kDa, and human 293T cells almost exclusively produced the 33,000-kDa form [1]. Notably, the two forms were found to have distinct activities, namely, full-length Cerberus antagonized Wnt, Nodal, and BMP signaling, whereas the short form only antagonized Nodal function [1]. We found that CHO cells also produced two forms of human Cerberus, a full-length form and a short form. The two forms also differed by approximately 10–15 kDa. As the short form of Cerberus appears to exist in different species (frog and human), we speculated that posttranslational processing could play a role in regulating Cerberus function. Sequence analysis of different Cerberus genes identified a conserved proprotein convertase processing site in mammalian Cerberus (amino acids 80–86 for human Cerberus; Fig. 1, RGFR|F; amino acids 125–128 for frog Cerberus, RRSFDKR|N) [29]. Remarkably, frog Cerberus also has a predicted proprotein convertase processing site near the engineered xCer-S N-terminus. As mutation of a key arginine (Arg81) in the human Cerberus proprotein convertase recognition motif significantly reduced proteolysis and as a construct lacking the N-terminal sequence produced a biologically active protein that migrated on SDS-PAGE electrophoresis with a molecular weight corresponding to the processed form, we speculate that the short form of Cerberus can be obtained by proprotein convertase processing at the predicted proprotein convertase processing site.

To determine if the two forms of human Cerberus are functionally distinct, we compared their abilities to bind ligands and inhibit signaling. In contrast to frog Cerberus, we found that the two human Cerberus forms bound ligands more or less equally (Figs. 2 and 3). However, they differed in their ability to block ligand binding to type II receptors. Full-length Cerberus effectively inhibited ligand binding to ActRIIA, ActRIIB, and BMPRII, whereas a far higher concentration of the short form was needed to achieve comparable inhibition (Fig. 4). As we previously demonstrated that Cerberus blocked Nodal binding to both type I and type II receptors, as well as to the co-receptor Cripto-1 [15], we propose that the principal molecular function of the short-form Cerberus fragment is to block the type I receptor and Cripto-1 binding sites (Fig. 6c and Fig. S2). By contrast, the cleavable N-terminal region does not contribute much to ligand binding affinity, but it improves blockade of the type II receptor binding site. As the different Cerberus-Fc constructs inhibited signaling equivalently, our findings support the conclusion that inhibition of the ligand–type I receptor interaction is sufficient for Cerberus to inhibit signaling by its cognate TGF- $\beta$  family ligands (Fig. 5). This inhibition directly correlates with ligand binding affinity.

Strikingly, full-length Cerberus profoundly suppressed migration of MDA-MB-231 breast cancer cells, whereas the short form largely lacked this activity (Fig. 6a and b). This puzzling finding could indicate that the suppressive effect of Cerberus on aggressive phenotypes of certain human breast cancer cell lines requires simultaneous inhibition of ligand binding to both type I and type II receptors [15]. Alternatively, the suppressive effect of Cerberus may not be due to inhibition of TGF- $\beta$  family signaling. Instead, the N-terminal region could have roles beyond the TGF- $\beta$  family, including inhibition of Wnt signaling [1]. However, whether mammalian Cerberus inhibits Wnt signaling is not certain. After the initial characterization of frog Cerberus [1], follow-up studies that combined mouse Cerberus and frog Wnt ligands could not reproduce this effect [13]. As the N-terminal region of frog and mouse Cerberus share less than 18% sequence identity, we propose that a frog Wnt ligand that interacts with frog Cerberus will not necessarily interact with mouse



Cerberus. Thus, whether mammalian Cerberus inhibits Wnt signaling by binding Wnt ligands has been neither demonstrated nor disproved. Our findings that other TGF- $\beta$  family signaling inhibitors, including the decoy receptors ActRIIA-Fc, ActRIIB-Fc, BMPRII-Fc, and TGF $\beta$ RII-Fc [28,30,31], and the small molecule type I receptor kinase inhibitor SB-431542 [32,33], failed to suppress MDA-MB-231 migration suggests that Cerberus inhibition of aggressive breast cancer cell phenotypes is complex and may also involve signaling pathways that do not belong to the TGF- $\beta$  family (Fig. S3). In future studies, we will investigate whether human Cerberus inhibits Wnt ligands or other signaling pathways in aggressive breast cancer cells.

## Materials and Methods

### Ligands

Recombinant human Activin A<sup>RnD/LT</sup> (P08476), Activin B<sup>RnD</sup> (Q53T31), GDF-8<sup>RnD</sup> (O08689), Nodal<sup>RnD</sup> (Q96S42), TGF- $\beta$ 1<sup>RnD</sup> (P01137), TGF- $\beta$ 2<sup>PC</sup> (P61812), TGF- $\beta$ 3<sup>PC</sup> (P10600), GDF-1<sup>RnD</sup> (NP\_001483), GDF-3<sup>RnD</sup> (Q9NR23), BMP-2<sup>LT</sup> (P12643), BMP-4<sup>LT</sup> (Q53XC5), BMP-6<sup>PC</sup> (P22004), BMP-7<sup>PC</sup> (P18075), BMP-9<sup>PC</sup> (Q9UK05), and BMP-10<sup>PC</sup> (O95393) were obtained from R&D Biosystems (RnD), Life Technologies (LT), or PROMOCCELL (PC). National Center for Biotechnology Information protein accession numbers are shown in parentheses. Activin A, GDF-8, and TGF- $\beta$ 1 were also produced in-house. BMP-2 was also obtained as a gift from Dr. Vicky Rosen.

### Expression plasmids

Synthetic genes consisting of human Cerberus (O95813), ActRIIA (P27037), and ActRIIB (Q13705) fused to human IgG1-Fc genes were obtained from GeneArt. Human BMPRII (Q13873) was cloned from cDNA and fused to human IgG1-Fc by PCR. National Center for Biotechnology Information protein accession numbers are shown in parentheses. Cerberus fusion constructs included the full-length gene (1–267, wtCer), a full-length construct with two mutations (1–267, R82G and C206A, mutCer), and a truncated form (1–17 83–267, C206A, CerS). Mutants and deletions were obtained by PCR. Receptor fusion constructs included extracellular domains of human ActRIIA (1–120), ActRIIB (1–120), and BMPRII (1–136). Extracellular domains were linked to human IgG1-Fc via a linker that is 22 amino acids long containing a TEV cleavage site.

### Protein purification

Proteins were expressed using CHO cells. wtCer-Fc, mutCer-Fc, CerS-Fc, ActRIIA-Fc, ActRIIB-Fc, and BMPRII-Fc were purified from condition medium using protein A capture. Proteins were eluted with 100 mM glycine (pH 3.0) and immediately neutralized by adding 10% (v/v) 2 M Tris (pH 8.5). To evaluate monodispersity, we analyzed proteins by SEC. For inhibition assays, the Fc portion of Cerberus constructs was removed using TEV protease. Cleaved Fc was removed with one step of protein A capture, followed by SEC. Purified proteins were dialyzed into phosphate-buffered saline (pH 7.5) and stored at  $-20^{\circ}\text{C}$  or  $-80^{\circ}\text{C}$ . The purity of the proteins was checked with SDS-PAGE under reducing and non-reducing conditions.

## Surface plasmon resonance

Ligand binding affinities and binding inhibition were determined by SPR using the Biacore 2000. All experiments were carried out at 25 °C. HBS-EPS buffer [0.01 M Hepes, 0.5 M NaCl, 3 mM ethylenediaminetetraacetic acid, and 0.005% (v/v) Tween 20 (pH 7.4)] containing 0.1% bovine serum albumin (Sigma-Aldrich) was used as running buffer. To capture Fc fusion proteins, including wtCer-Fc, mutCer-Fc, CerS-Fc, ActRIIA-Fc, ActRIIB-Fc, and BMPRII-Fc, we immobilized anti-human IgG (Fc) antibody onto four channels of a CM5 chip using amine-coupling chemistry. To characterize ligand binding specificity of Cerberus, we injected different ligands at a concentration of 80 nM, including Nodal, Activin A, Activin B, GDF-8, GDF-11, TGF- $\beta$ 1, TGF- $\beta$ 2, TGF- $\beta$ 3, BMP-2, BMP-6, BMP-7, BMP-9, and BMP-10. For kinetic analysis of ligands that bound Cerberus (Nodal, Activin B, BMP-6, and BMP-7), a series of concentrations was injected over experimental and control flow channels. To minimize mass transport artifacts, we used a high flow rate (50  $\mu$ l/min) and captured low levels of purified wtCer-Fc, mutCer-Fc, or CerS-Fc (approximately 200–300 RU) on the experimental flow channels. A reference channel was monitored to account for nonspecific binding, drift, and bulk shifts. To obtain kinetic rate constants, we fitted the processed data to a 1:1 Langmuir interaction model with mass transport limitation using BiaEvaluation software. By including a mass transport term into the Langmuir 1:1 binding model, we were able to achieve an excellent fit of the experimental data as shown by overlay of the simulated binding responses (black lines). BiaEvaluation software calculated binding rate constants ( $k_a$  and  $k_d$ ), mass transport rate constant ( $k_t$ ), and confidence errors ( $\chi^2$ ). Equilibrium dissociation constants ( $K_d$ ) were determined by calculating the ratio of binding rate constants. Results are summarized in Table 1. A detailed kinetic evaluation model is described in the supplemental materials. After each binding cycle, the antibody surface was regenerated to base line by injecting 3 M MgCl<sub>2</sub>. For SPR inhibition analysis, ActRIIA-Fc, ActRIIB-Fc, or BMPRII-Fc was captured on the sensor chip. Activin B and BMP-6 at certain concentration were preincubated with different concentrations of Fc free wtCer, mutCer, or CerS. Preformed complexes were injected over experimental and control flow channels. Sensograms were analyzed by double referencing. IC<sub>50</sub> values for SPR inhibition data were determined using GraphPad. Results are summarized in Table 2. After each binding cycle, the antibody surface was regenerated to base line by injecting 3 M MgCl<sub>2</sub>.

## Cell lines

A-204 rhabdomyosarcoma cells (HTB-82) and HepG2 cells (HB-8065) were obtained from ATCC. Cells were maintained according to ATCC (American Type Culture Collection) culture conditions. A-204 cells were grown in McCoy's 5A medium supplemented with 10% fetal bovine serum and 1% penicillin/streptavidin. HepG2 cells were grown in Eagle's minimum essential medium supplemented with 10% fetal bovine serum and 1% penicillin/streptavidin. Cells were grown at 37 °C under humidified, 5% CO<sub>2</sub> atmosphere. Freshly thawed cells were passaged at least three times before performing assays.

## Reporter assays

A total of ~50,000 A-204 or ~10,000 HepG2 cells in complete medium were seeded in each well of a 96-well plate and grown overnight. For transfection, solutions containing 24  $\mu$ l lipofectamine 2000, assay medium (960  $\mu$ l growth medium supplemented with 0.1% bovine serum albumin), 192 ng Pgl4.48 [Luc2P/hRluc/TK] vector (control luciferase reporter plasmid; Promega, E6921), and 19.2  $\mu$ g of the SMAD3 responsive reporter plasmid pGL4.48 [luc2P/SBE] or the SMAD1/5/8 responsive reporter plasmid pGL3 [luc2P/BRE] were prepared and incubated at room temperature for 30 min. After incubation, 3840  $\mu$ l assay medium was added to the transfection solutions, and 50  $\mu$ l of this mixture was added to each well. Transfection medium was removed the following day, and medium was replaced with assay medium containing test proteins, including Activin A, Activin B, and BMP-6 (all 10 ng/ml) and/or the Cerberus-Fc constructs (0–10,000 ng/ml). Assay medium containing test proteins was incubated at 37 °C for 1 h before adding to cells. After addition of medium, A-204 cells were incubated for 6 h and HepG2 cells were incubated for 16 h at 37 °C, and luciferase activity was detected with the Dual-Glo Luciferase Assay System (Promega) or a homemade version of that assay [34]. Luminescence was determined using an FluoStar Omega plate reader. Relative luciferase units (RLU) were calculated by dividing firefly luciferase units (fLU) with renilla luciferase units (rLU). IC<sub>50</sub> values were determined using GraphPad. Results are summarized in Table 2.

## Wound healing

MDA-MB-231 human breast cancer cells (ATCC HTB-26) were seeded in an Ibidi insert in standard growth medium. Once cells reached 80% confluence, the insert was removed and medium was replaced with complete medium containing 2.5  $\mu$ g/ml mitomycin C and 17.8 nM wtCer-Fc, mutCer-Fc CerS-Fc, or no Cerberus control. Cells were monitored for up to 24 h and images were taken using an inverted microscope with a magnification of 10 $\times$  at 0 h and 24 h. Cellular migration was quantified using Vimages software (Ibidi).

## Statistics

Reporter gene assays were performed in quadruplicates and were repeated two different times. Statistical significance was determined by comparing control to treated sample using a two-tailed *T* test. *P* values <0.05 were considered statistically significant and are marked by an asterisk in Fig. 5.

## Supplementary Material

Refer to Web version on PubMed Central for supplementary material.

## Acknowledgements

We would like to thank Dr. Washington Mutatu and Dr. Stacy Hovde for constructing expression vectors, Jake Reske and Wendi Ni for assistance with protein purification, and Michigan State University and the Clinical and Translational Science Institute for financial support.

## Abbreviations used:

<b>SPR</b>	surface plasmon resonance
<b>SEC</b>	size-exclusion chromatography
<b>CerS</b>	short Cerberus
<b>TGF-<math>\beta</math></b>	transforming growth factor- $\beta$
<b>GDF</b>	growth and differentiation factor
<b>BMD</b>	bone mineral density
<b>CHO</b>	Chinese hamster ovary

## References

- [1]. Piccolo S, Agius E, Leyns L, Bhattacharyya S, Grunz H, Bouwmeester T, De Robertis EM, The head inducer Cerberus is a multifunctional antagonist of Nodal, BMP and Wnt signals, *Nature* 397 (1999) 707–710. [PubMed: 10067895]
- [2]. Nolan K, Thompson TB, The DAN family: Modulators of TGF-beta signaling and beyond, *Protein Sci.* 23 (2014) 999–1012. [PubMed: 24810382]
- [3]. Bouwmeester T, Kim S, Sasai Y, Lu B, De Robertis EM, Cerberus is a head-inducing secreted factor expressed in the anterior endoderm of Spemann’s organizer, *Nature* 382 (1996) 595–601. [PubMed: 8757128]
- [4]. Foley AC, Gupta RW, Guzzo RM, Korol O, Mercola M, Embryonic heart induction, *Ann. N. Y. Acad. Sci.* 1080 (2006) 85–96. [PubMed: 17132777]
- [5]. Zhu L, Marvin MJ, Gardiner A, Lassar AB, Mercola M, Stern CD, Levin M, Cerberus regulates left-right asymmetry of the embryonic head and heart, *Curr. Biol.* 9 (1999) 931–938. [PubMed: 10508582]
- [6]. Perea-Gomez A, Vella FD, Shawlot W, Oulad-Abdelghani M, Chazaud C, Meno C, Pfister V, Chen L, Robertson E, Hamada H, Behringer RR, Ang SL, Nodal antagonists in the anterior visceral endoderm prevent the formation of multiple primitive streaks, *Dev. Cell* 3 (2002) 745–756. [PubMed: 12431380]
- [7]. Cai W, Albin S, Wei K, Willems E, Guzzo RM, Tsuda M, Giordani L, Spiering S, Kurian L, Yeo GW, Puri PL, Mercola M, Coordinate Nodal and BMP inhibition directs Baf60c-dependent cardiomyocyte commitment, *Genes Dev.* 27 (2013) 2332–2344. [PubMed: 24186978]
- [8]. Foley AC, Korol O, Timmer AM, Mercola M, Multiple functions of Cerberus cooperate to induce heart downstream of Nodal, *Dev. Biol.* 303 (2007) 57–65. [PubMed: 17123501]
- [9]. Glinka A, Wu W, Onichtchouk D, Blumenstock C, Niehrs C, Head induction by simultaneous repression of Bmp and Wnt signalling in *Xenopus*, *Nature* 389 (1997) 517–519. [PubMed: 9333244]
- [10]. Koromila T, Dailiana Z, Samara S, Chassanidis C, Tzavara C, Patrinos GP, Aleporou-Marinou V, Kollia P, Novel sequence variations in the CER1 gene are strongly associated with low bone mineral density and risk of osteoporotic fracture in postmenopausal women, *Calcif. Tissue Int.* 91 (2012) 15–23. [PubMed: 22543871]
- [11]. Koromila T, Georgoulas P, Dailiana Z, Ntzani EE, Samara S, Chassanidis C, Aleporou-Marinou V, Kollia P, CER1 gene variations associated with bone mineral density, bone markers, and early menopause in postmenopausal women, *Hum. Genomics* 7 (2013) 21. [PubMed: 24138842]
- [12]. Tang PL, Cheung CL, Sham PC, McClurg P, Lee B, Chan SY, Smith DK, Tanner JA, Su AI, Cheah KS, Kung AW, Song YQ, Genome-wide haplotype association mapping in mice identifies a genetic variant in CER1 associated with BMD and fracture in southern Chinese women, *J. Bone Miner. Res.* 24 (2009) 1013–1021. [PubMed: 19113921]

- [13]. Belo JA, Bachiller D, Agius E, Kemp C, Borges AC, Marques S, Piccolo S, De Robertis EM, Cerberus-like is a secreted BMP and nodal antagonist not essential for mouse development, *Genesis* 26 (2000) 265–270. [PubMed: 10748465]
- [14]. Belo JA, Silva AC, Borges AC, Filipe M, Bento M, Goncalves L, Vitorino M, Salgueiro AM, Teixeira V, Tavares AT, Marques S, Generating asymmetries in the early vertebrate embryo: The role of the Cerberus-like family, *Int. J. Dev. Biol.* 53 (2009) 1399–1407. [PubMed: 19247954]
- [15]. Aykul S, Ni W, Mutatu W, Martinez-Hackert E, Human Cerberus prevents Nodal-receptor binding, inhibits Nodal signaling, and suppresses Nodal-mediated phenotypes, *PLoS One* 10 (2015) e0114954. [PubMed: 25603319]
- [16]. Nolan K, Kattamuri C, Luedeke DM, Deng X, Jagpal A, Zhang F, Linhardt RJ, Kenny AP, Zorn AM, Thompson TB, Structure of protein related to Dan and Cerberus: Insights into the mechanism of bone morphogenetic protein antagonism, *Structure* 21 (2013) 1417–1429. [PubMed: 23850456]
- [17]. Nolan K, Kattamuri C, Luedeke DM, Angerman EB, Rankin SA, Stevens ML, Zorn AM, Thompson TB, Structure of neuroblastoma suppressor of tumorigenicity 1 (NBL1): Insights for the functional variability across bone morphogenetic protein (BMP) antagonists, *J. Biol. Chem.* 290 (2015) 4759–4771. [PubMed: 25561725]
- [18]. Hsu DR, Economides AN, Wang X, Eimon PM, Harland RM, The *Xenopus* dorsalizing factor Gremlin identifies a novel family of secreted proteins that antagonize BMP activities, *Mol. Cell* 1 (1998) 673–683. [PubMed: 9660951]
- [19]. Harada K, Shintani Y, Sakamoto Y, Wakatsuki M, Shitsukawa K, Saito S, Serum immunoreactive activin A levels in normal subjects and patients with various diseases, *J. Clin. Endocrinol. Metab.* 81 (1996) 2125–2130. [PubMed: 8964839]
- [20]. Suragani RN, Cadena SM, Cawley SM, Sako D, Mitchell D, Li R, Davies MV, Alexander MJ, Devine M, Loveday KS, Underwood KW, Grinberg AV, Quisel JD, Chopra R, Pearsall RS, Seehra J, Kumar R, Transforming growth factor-beta superfamily ligand trap ACE-536 corrects anemia by promoting late-stage erythropoiesis, *Nat. Med.* 20 (2014) 408–414. [PubMed: 24658078]
- [21]. Kropf J, Schurek JO, Wollner A, Gressner AM, Immunological measurement of transforming growth factor-beta 1 (TGF-beta1) in blood; assay development and comparison, *Clin. Chem.* 43 (1997) 1965–1974. [PubMed: 9342020]
- [22]. Kumar A, Novoselov V, Celeste AJ, Wolfman NM, ten Dijke P, Kuehn MR, Nodal signaling uses activin and transforming growth factor-beta receptor-regulated Smads, *J. Biol. Chem.* 276 (2001) 656–661. [PubMed: 11024047]
- [23]. Chen Y, Lebrun JJ, Vale W, Regulation of transforming growth factor beta- and activin-induced transcription by mammalian Mad proteins, *Proc. Natl. Acad. Sci. U. S. A.* 93 (1996) 12992–12997. [PubMed: 8917532]
- [24]. Nakao A, Imamura T, Souchelnytskyi S, Kawabata M, Ishisaki A, Oeda E, Tamaki K, Hanai J, Heldin CH, Miyazono K, ten Dijke P, TGF-beta receptor-mediated signalling through Smad2, Smad3 and Smad4, *EMBO J.* 16 (1997) 5353–5362. [PubMed: 9311995]
- [25]. Korchynskyi O, ten Dijke P, Identification and functional characterization of distinct critically important bone morphogenetic protein-specific response elements in the Id1 promoter, *J. Biol. Chem.* 277 (2002) 4883–4891. [PubMed: 11729207]
- [26]. Zawel L, Dai JL, Buckhaults P, Zhou S, Kinzler KW, Vogelstein B, Kern SE, Human Smad3 and Smad4 are sequence-specific transcription activators, *Mol. Cell* 1 (1998) 611–617. [PubMed: 9660945]
- [27]. Walsh DW, Godson C, Brazil DP, Martin F, Extracellular BMP-antagonist regulation in development and disease: Tied up in knots, *Trends Cell Biol.* 20 (2010) 244–256. [PubMed: 20188563]
- [28]. Pearsall RS, Canalis E, Cornwall-Brady M, Underwood KW, Haigis B, Ucran J, Kumar R, Pobre E, Grinberg A, Werner ED, Glatt V, Stadmeier L, Smith D, Seehra J, Boussein ML, A soluble activin type IIA receptor induces bone formation and improves skeletal integrity, *Proc. Natl. Acad. Sci. U. S. A.* 105 (2008) 7082–7087. [PubMed: 18460605]

- [29]. Duckert P, Brunak S, Blom N, Prediction of proprotein convertase cleavage sites, *Protein Eng. Des. Sel.* 17 (2004) 107–112. [PubMed: 14985543]
- [30]. Lee SJ, Reed LA, Davies MV, Girgenrath S, Goad ME, Tomkinson KN, Wright JF, Barker C, Ehrmantraut G, Holmstrom J, Trowell B, Gertz B, Jiang MS, Sebald SM, Matzuk M, Li E, Liang LF, Quattlebaum E, Stotish RL, Wolfman NM, Regulation of muscle growth by multiple ligands signaling through activin type II receptors, *Proc. Natl. Acad. Sci. U. S. A.* 102 (2005) 18117–18122. [PubMed: 16330774]
- [31]. Kim MY, Oskarsson T, Acharyya S, Nguyen DX, Zhang XH, Norton L, Massague J, Tumor self-seeding by circulating cancer cells, *Cell* 139 (2009) 1315–1326. [PubMed: 20064377]
- [32]. Inman GJ, Nicolas FJ, Callahan JF, Harling JD, Gaster LM, Reith AD, Laping NJ, Hill CS, SB-431542 is a potent and specific inhibitor of transforming growth factor-beta superfamily type I activin receptor-like kinase (ALK) receptors ALK4, ALK5, and ALK7, *Mol. Pharmacol.* 62 (2002) 65–74. [PubMed: 12065756]
- [33]. Laping NJ, Grygielko E, Mathur A, Butter S, Bomberger J, Tweed C, Martin W, Fornwald J, Lehr R, Harling J, Gaster L, Callahan JF, Olson BA, Inhibition of transforming growth factor (TGF)-beta1-induced extracellular matrix with a novel inhibitor of the TGF-beta type I receptor kinase activity: SB-431542, *Mol. Pharmacol.* 62 (2002) 58–64. [PubMed: 12065755]
- [34]. Baker JM, Boyce FM, High-throughput functional screening using a homemade dual-glow luciferase assay, *J. Vis. Exp.* (2014), 10.3791/50282.

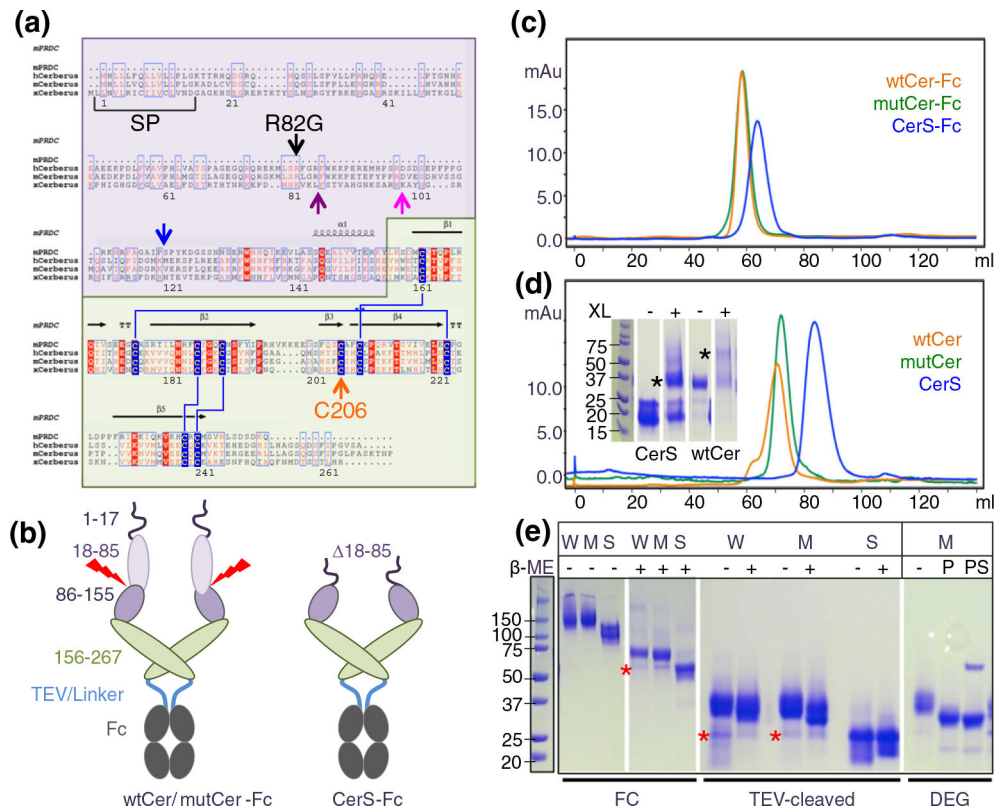


**Fig. 1.** Construct design and purification. (a) Multiple sequence alignment of the DAN family proteins PRDC (mouse) and Cerberus (human, mouse, and frog). DAN family proteins are secreted regulators of TGF- $\beta$  family signaling that have a signal peptide for secretion (SP) and a conserved cystine knot domain (highlighted in green, Cerberus amino acids 156–267). Cerberus has a unique N-terminal region of unknown function (highlighted in purple, Cerberus amino acids 19–155). Cerberus molecules are posttranslationally processed and have a predicted proprotein convertase processing site, marked by the purple arrow for mammalian Cerberus and by a blue arrow for frog Cerberus [29], or a proposed processing site marked by a pink arrow [1]. Cerberus molecules also have an unpaired cysteine (Cys206 in human Cerberus, orange arrow). Arginine 82 and cysteine 206 were mutated for functional analysis. (b) Domain organization of Cerberus and construct design. Cerberus consists of three distinct regions, the cleavable N-terminal region (amino acids 19–85, light purple), the residual N-terminal region (amino acids 86–155, dark purple), and the cystine knot domain (amino acids 156–267, green). Three different constructs were created: Full-length human Cerberus with the wild-type sequence (wtCer-Fc), full-length Cerberus with mutations at arginine 82 and cysteine 206 (mutCer-Fc), and a short form lacking the N-terminal region (amino acids 18–85) and mutated at cysteine 206 (CerS-Fc). Cerberus genes were fused at the C-terminus to human IgG1-Fc via a 22-amino-acid linker containing a TEV cleavage site. (c) Purification of wtCer-Fc, mutCer-Fc, and CerS-Fc expressed in CHO cells. Following two purification steps, molecules migrate as a single, well-defined peak in a size-exclusion chromatographic column. The molecular weight of each protein corresponds to the dimeric species. (d) Purification of wtCer, mutCer, and CerS after removal of the Fc

domain. All molecules migrate as a single, well-defined peak in a SEC column. For wtCer and mutCer, the molecular weight corresponds to the dimeric species. CerS elutes at a volume that corresponds to a monomeric form, but it also forms dimers in solution. The inserted SDS-PAGE shows glutaraldehyde cross-linking of CerS. The dimeric CerS is highlighted by the black asterisk. For functional studies, only the main peak fractions were used and fractions corresponding to higher-molecular-weight species were discarded. (e) SDS-PAGE gels of purified proteins. The two left panels show non-reducing ( $-\beta$ -ME) and reducing ( $+\beta$ -ME) SDS-PAGE gels of the Fc fusion forms (W: wtCer-Fc, M: mutCer-Fc, S: CerS-Fc). Expected molecular masses are 57 kDa for wtCer-Fc, 57 kDa for mutCer-Fc, and 49 kDa for CerS-Fc. Higher apparent molecular weights are due to glycosylation. wtCer-Fc and mutCer-Fc have three N-linked glycosylation sites per protomer, two in the Cerberus moiety and one in the Fc moiety. CerS-Fc has two N-linked glycosylation sites per protomer, one in the Cerberus moiety and one in the Fc moiety. Fc fusion constructs form disulfide-linked dimers via the Fc domain. The two right panels show Fc free Cerberus. The molecular weights of the three cleaved Cerberus constructs correspond to a monomeric form under reducing and non-reducing conditions. Deglycosylation with PNGase F alone (P) or with PNGase F and sialidase (PS) reduces the molecular weight of mutant Cerberus to the theoretically expected value. The red star designates processed Cerberus.



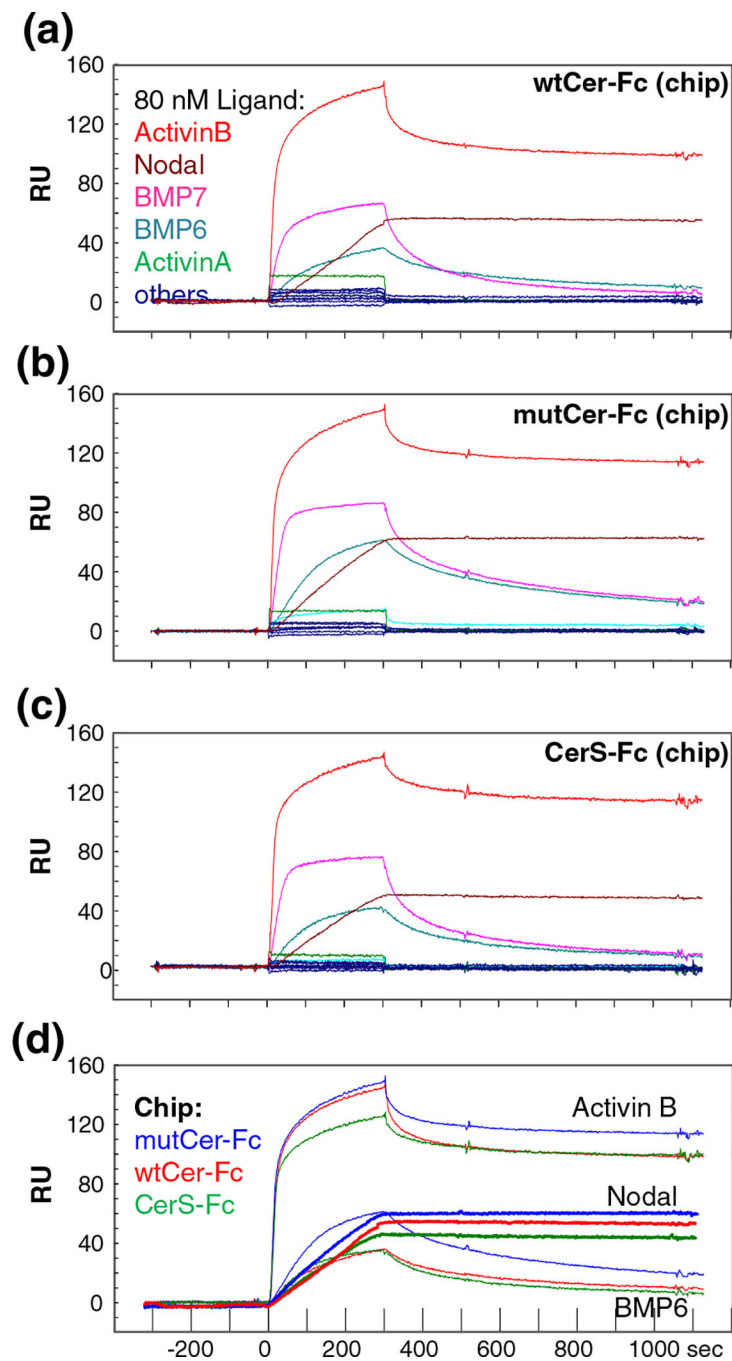


**Fig. 2.** Cerberus ligand binding comparison. Ligand binding comparison of (a) wtCer-Fc, (b) mutCer-Fc, and (c) CerS-Fc. Equal amounts of wtCer-Fc, mutCer-Fc, and CerS-Fc were captured on the SPR sensor chip and different ligands were injected over them at 80 nM concentration. Activin B (red), Nodal (maroon), BMP-6 (teal), and BMP-7 (pink) bind wtCer-Fc, mutCer-Fc, and CerS-Fc with high affinity. All other tested ligands did not bind Cerberus. (d) Comparison of Activin B, Nodal, and BMP-6 binding to wtCer-Fc, mutCer-Fc, and CerS-Fc. Equal amounts of wtCer-Fc, mutCer-Fc, and CerS-Fc were immobilized on

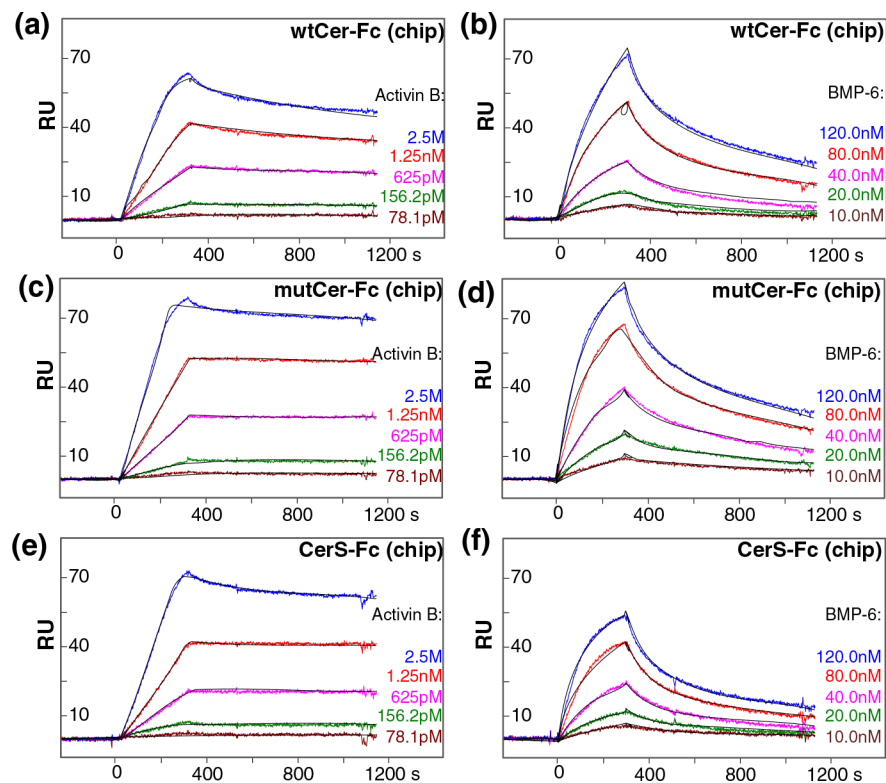
SPR sensor chip, and 80 nM Activin B, Nodal, or BMP-6 was injected. wtCer-Fc (red curves), mutCer-Fc (blue curves), and CerS-Fc (green curves) show very similar binding profiles.

Author Manuscript

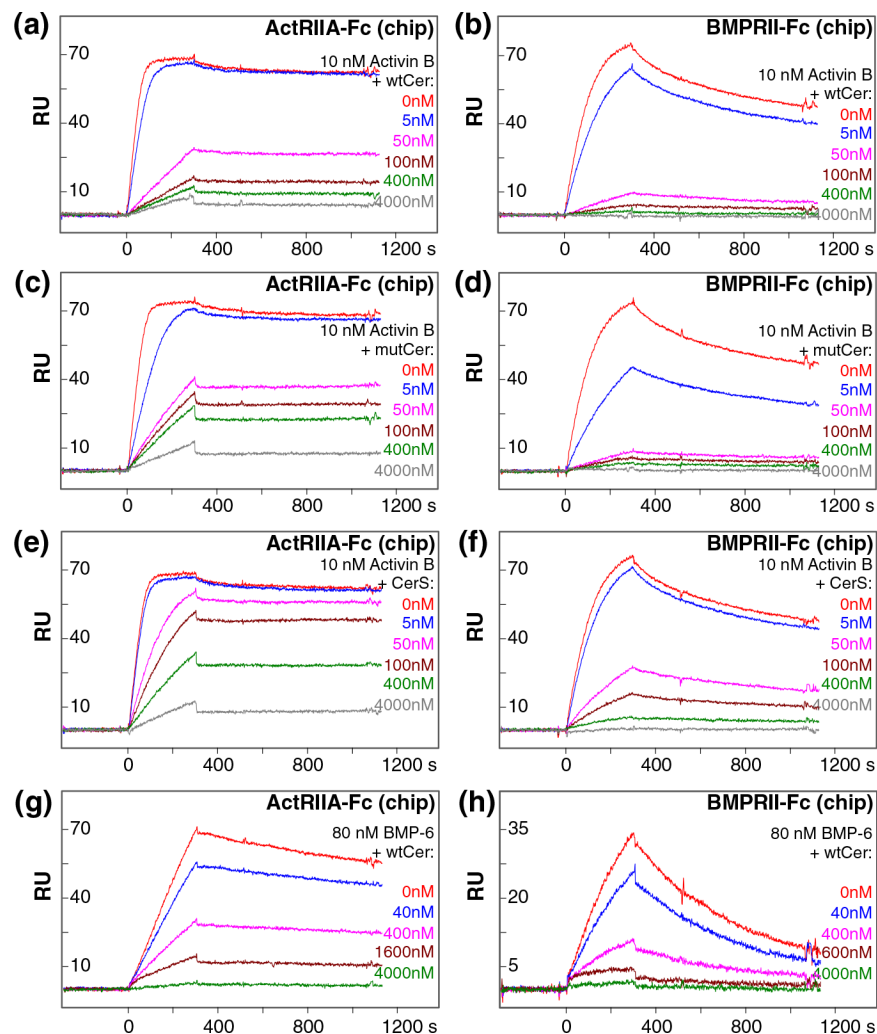
Author Manuscript

Author Manuscript

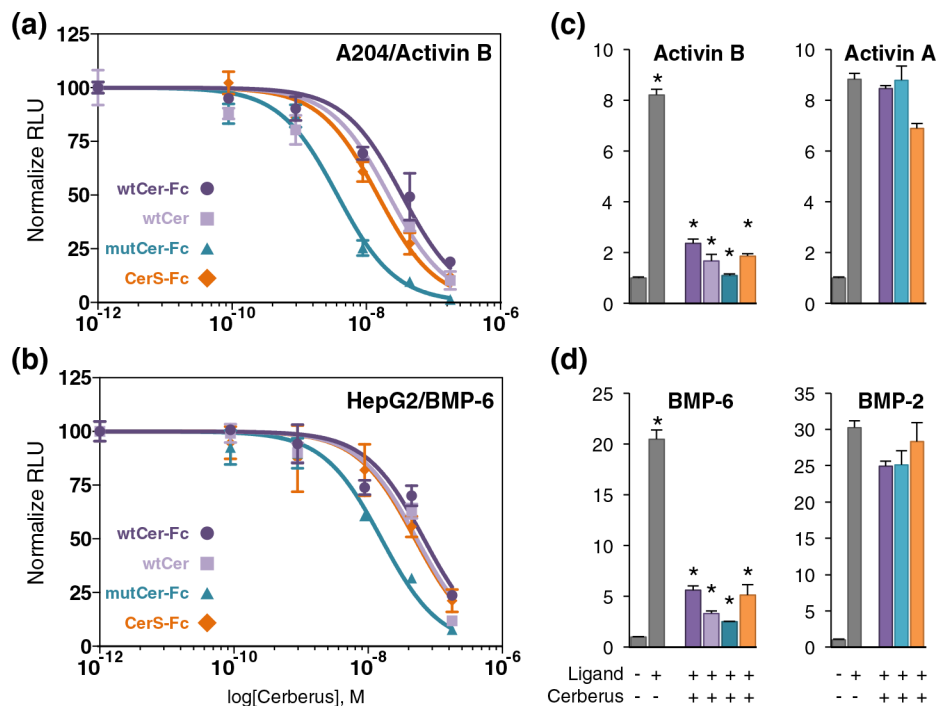
Author Manuscript



**Fig. 3.** Cerberus ligand binding affinities. (a) Activin B–wtCer-Fc interaction. wtCer-Fc was immobilized on the SPR sensor chip and different concentrations of Activin B were injected as shown. The estimated Activin B–wtCer-Fc association constant ( $k_a$ ) is  $2.3 \times 10^6 \text{ M}^{-1} \text{ s}^{-1}$ , the dissociation constant ( $k_d$ ) is  $2.2 \times 10^{-4} \text{ s}^{-1}$ , and the equilibrium dissociation constant ( $K_d$ ) is 0.096 nM. (b) Activin B–mutCer-Fc interaction. mutCer-Fc was immobilized and Activin B was injected as shown. The estimated Activin B–mutCer-Fc association constant ( $k_a$ ) is  $2.0 \times 10^6 \text{ M}^{-1} \text{ s}^{-1}$ , the dissociation constant ( $k_d$ ) is  $3.1 \times 10^{-5} \text{ s}^{-1}$ , and the equilibrium dissociation constant ( $K_d$ ) is 0.016 nM. (c) Activin B–CerS-Fc interaction. CerS-Fc was immobilized and Activin B was injected. The estimated Activin B–CerS-Fc association constant ( $k_a$ ) is  $1.2 \times 10^6 \text{ M}^{-1} \text{ s}^{-1}$ , the dissociation constant ( $k_d$ ) is  $1.7 \times 10^{-5} \text{ s}^{-1}$ , and the equilibrium dissociation constant ( $K_d$ ) is 0.014 nM. (d) BMP-6–wtCer-Fc interaction. wtCer-Fc was immobilized and BMP-6 was injected. The estimated BMP-6–wtCer-Fc association constant ( $k_a$ ) is  $5.5 \times 10^4 \text{ M}^{-1} \text{ s}^{-1}$ , the dissociation constant ( $k_d$ ) is  $1.1 \times 10^{-3} \text{ s}^{-1}$ , and the equilibrium dissociation constant ( $K_d$ ) is 19 nM. (e) BMP-6–mutCer-Fc interaction. mutCer-Fc was immobilized and BMP-6 was injected. The estimated BMP-6–mutCer-Fc association constant ( $k_a$ ) is  $6.9 \times 10^4 \text{ M}^{-1} \text{ s}^{-1}$ , the dissociation constant ( $k_d$ ) is  $1.0 \times 10^{-3} \text{ s}^{-1}$ , and the equilibrium dissociation constant ( $K_d$ ) is 15 nM. (f) BMP-6–CerS-Fc interaction. CerS-Fc was immobilized BMP-6 was injected. The estimated BMP-6–CerS-Fc association constant ( $k_a$ ) is  $8.2 \times 10^4 \text{ M}^{-1} \text{ s}^{-1}$ , the dissociation constant ( $k_d$ ) is  $1.2 \times 10^{-3} \text{ s}^{-1}$ , and the equilibrium dissociation constant ( $K_d$ ) is 15 nM. (a–f) Fitted curves (black lines) are superimposed over all experimental curves.



**Fig. 4.** Cerberus inhibition of ligand–type II receptor interactions. (a) wtCer inhibition of Activin B–ActRIIA binding. (b) wtCer inhibition of Activin B–BMPRII binding. (c) mutCer inhibition of Activin B–ActRIIA binding. (d) mutCer inhibition of Activin B–BMPRII binding. (e) CerS inhibition of Activin B–ActRIIA binding. (f) CerS inhibition of Activin B–BMPRII binding. (g) wtCer inhibition of BMP-6–ActRIIA binding. (h) wtCer inhibition of BMP-6–BMPRII binding. ActRIIA-Fc or BMPRII-Fc was immobilized on the SPR sensor chip. (a–f) Activin B (10 nM) was preincubated with 0 nM (red), 5 nM (blue), 50 nM (magenta), 100 nM (brown), 400 nM (green), and 4000 nM (gray) wtCer, mutCer, or CerS. Preformed Activin B–Cerberus complexes were injected over the sensor chip. (g and h) BMP-6 (80 nM) was preincubated with 0 nM (red), 40 nM (blue), 400 nM (magenta), 1600 nM (brown), and 4000 nM (green) wtCer. Preformed BMP-6–Cerberus complexes were injected over the sensor chip. (a–h) wtCer, mutCer, and CerS prevent binding of Activin B and BMP-6 to type II receptors ActRIIA and BMPRII, as seen in the almost complete loss of SPR response at the 4000 nM Cerberus concentration.

**Fig. 5.**

Cerberus inhibition of SMAD2/3 and SMAD1/5/8 signaling. (a) SMAD2/3 signaling inhibition. A-204 cells were transfected with SMAD3 responsive reporter and control plasmids. Cells were treated with 0.8 nM Activin B, as well as wtCer-Fc (dark purple)/wtCer (light purple), mutCer-Fc (dark blue), or CerS-Fc (dark orange). Cerberus concentrations were (1) 0.089 nM, (2) 0.89 nM, (3) 8.9 nM, (4) 44.5 nM, and (5) 178 nM. (b) SMAD1/5/8 signaling inhibition. HepG2 cells were transfected with SMAD1/5/8 responsive reporter and control plasmids. Cells were treated with 0.8 nM BMP-6, as well as wtCer-Fc (dark purple)/wtCer (light purple), mutCer-Fc (dark blue), or CerS-Fc (dark orange). Cerberus concentrations were (1) 0.089 nM, (2) 0.89 nM, (3) 8.9 nM, (4) 44.5 nM, and (5) 178 nM. (c) Single point comparison of SMAD2/3 signaling inhibition by Cerberus in A-204 cells. Cells were treated with 0.8 nM Activin B (left panel) or Activin A (right panel), as well as 178 nM wtCer-Fc, wtCer, mutCer-Fc, or CerS-Fc. (d) Single point comparison of SMAD1/5/8 signaling inhibition by Cerberus in HepG2 cells. Cells were treated with 0.8 nM BMP-6 (left panel) or BMP-2 (right panel), as well as 178 nM wtCer-Fc, mutCer-Fc, or CerS-Fc. Signaling was detected as firefly luciferase activity and normalized against renilla luciferase activity. Relative luciferase units (RLU) were calculated by dividing firefly luciferase units (fLU) with renilla luciferase units (rLU). Data are expressed as mean + standard error of four independent measurements. Statistically significant differences calculated using a two-tailed *T* test are marked by an asterisk (\*) ( $P < 0.05$ ).

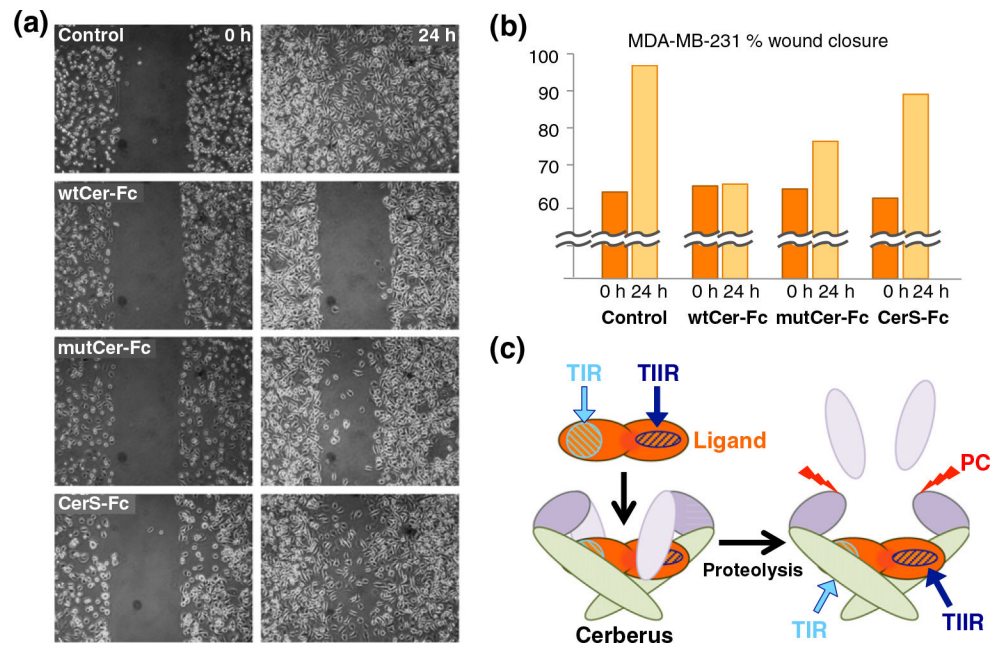


**Fig. 6.** Cerberus inhibition of breast cancer cell migration. (a) Inhibition of MDA-MB-231 wound closure by Cerberus. MDA-MB-231 breast cancer cells were plated in Ibidi insert dishes and grown to 80% confluence. Inserts were removed to create a gap and medium was exchanged with complete medium containing 2.5  $\mu\text{g/ml}$  mitomycin C and 0 nM (control) or 17.8 nM wtCer-Fc, mutCer-Fc, and CerS-Fc. Images were taken after insert removal (0 h) and after 24 h incubation with Cerberus (24 h). (b) Wound closure quantification. Images taken at 0 h and 24 h were analyzed using Wimasis software to quantify cellular migration. The dark-orange bar corresponds to image taken at 0 h, and the light-orange bar corresponds to image taken at 24 h. Control corresponds to experiment carried out without Cerberus. (c) Model of Cerberus function. Cerberus forms non-covalent dimers via the cystine knot domain (green, residues 156–267) [16,17]. The N-terminal domain has a propeptide cleavage site at amino acids 82–85 (cleavable region, residues 18–85, light purple; short domain region, residues 86–155, dark purple). TGF- $\beta$  family ligands bind two type I and two type II receptors to form active signaling complexes. Type II receptors bind the convex surface of a ligand (dark blue, striped oval), and type I receptors bind the concave surface of a ligand (light blue, striped circle). The N-terminal region of full-length Cerberus helps prevent type II receptor binding and thus may block the type II receptor binding site. Cerberus short inhibits signaling and thus likely blocks the type I receptor binding-site.

Table 1

Equilibrium dissociation and rate constants.

Flow	Chip	$k_a$	$k_d$	$K_d$
Activin B	wtCer-Fc	$(2.3 \pm 0.1) \times 10^6$	$(2.2 \pm 0.2) \times 10^{-4}$	$0.096 \pm 0.01$
	mutCer-Fc	$(2.0 \pm 0.3) \times 10^6$	$(3.1 \pm 0.2) \times 10^{-5}$	$0.016 \pm 0.003$
	CerS-Fc	$(1.2 \pm 0.2) \times 10^6$	$(1.7 \pm 0.1) \times 10^{-5}$	$0.014 \pm 0.002$
BMP-6	wtCer-Fc	$(5.5 \pm 1.4) \times 10^4$	$(1.1 \pm 0.2) \times 10^{-3}$	$19.1 \pm 2.5$
	mutCer-Fc	$(7.0 \pm 1.0) \times 10^4$	$(1.0 \pm 0.1) \times 10^{-3}$	$14.7 \pm 3.6$
	CerS-Fc	$(8.0 \pm 0.4) \times 10^4$	$(1.2 \pm 0.1) \times 10^{-3}$	$15.2 \pm 1.4$
BMP-7	wtCer-Fc	$(1.6 \pm 0.2) \times 10^5$	$(2.8 \pm 0.1) \times 10^{-3}$	$17.3 \pm 0.8$
	mutCer-Fc	$(1.3 \pm 0.5) \times 10^5$	$(1.2 \pm 0.1) \times 10^{-3}$	$9.8 \pm 0.9$
	CerS-Fc	$(1.4 \pm 0.2) \times 10^5$	$(2.1 \pm 0.2) \times 10^{-3}$	$15.6 \pm 1.9$

Units are presented in parentheses as follows:  $K_d$  ( $M^{-1} s^{-1}$ ),  $K_d$  (nM),  $\chi^2$  (RU<sup>2</sup>), and  $k_f$  [RU/(M s)]. Number of replicates:  $N = 3$ .

**Table 2.**

IC<sub>50</sub> values for SPR binding inhibition and reporter assays.

<i>SPR binding<sup>a</sup> [IC<sub>50</sub> (nM)]</i>				
Ligand	Chip	wtCer	mutCer	CerS
Activin B	ActRIIA	26.2 ± 1.7	40.1 ± 2.5	261.0 ± 33.2
Activin B	BMPRII	14.9 ± 4.2	7.4 ± 1.1	28.4 ± 9.6
BMP-6	ActRIIA	319.0 ± 53.4	350.0 ± 96.1	N.D.
BMP-6	BMPRII	156.0 ± 9.2	48.3 ± 3.5	N.D.
<i>Reporter signaling<sup>b</sup> [IC<sub>50</sub> (nM)]</i>				
Ligand	Cell line	wtCer-Fc	mutCer-Fc	CerS-Fc
Activin B	A-204	34.1 ± 9.4	3.7 ± 1.0	14.8 ± 1.1
BMP-6	HepG2	67.8 ± 24.0	15.8 ± 3.2	49.9 ± 11.8

Five inhibitor concentrations were used.

<sup>a</sup>Number of replicates: *N* = 3.

<sup>b</sup>Number of replicates: *N* = 4.